CHALMERS
UNIVERSITY OF TECHNOLOGY

Revealing the Hidden Spin-Polarized Bands in a Superconducting Tl Bilayer Crystal

Downloaded from: https://research.chalmers.se, 2025-12-04 14:01 UTC

Citation for the original published paper (version of record):
Kobayashi, T., Toichi, Y., Yaji, K. et al (2023). Revealing the Hidden Spin-Polarized Bands in a Superconducting Tl Bilayer Crystal. Nano Letters, 23(16): 7675-7682.
http://dx.doi.org/10.1021/acs.nanolett.3c02387

N.B. When citing this work, cite the original published paper.

research.chalmers.se offers the possibility of retrieving research publications produced at Chalmers University of Technology. It covers all kind of research output: articles, dissertations, conference papers, reports etc. since 2004. research.chalmers.se is administrated and maintained by Chalmers Library

(article starts on next page)

NANO LETTERS

pubs.acs.org/NanoLett

Letter

Revealing the Hidden Spin-Polarized Bands in a Superconducting Tl Bilayer Crystal

Takahiro Kobayashi, Yuichiro Toichi, Koichiro Yaji, Yoshitaka Nakata, Yuchi Yaoita, Mutsuki Iwaoka, Mariko Koga, Yituo Zhang, Jun Fujii, Shimpei Ono, Yasmine Sassa, Yasuo Yoshida, Yukio Hasegawa, Fumio Komori, Shik Shin, Satoru Ichinokura, Ryota Akiyama, Shuji Hasegawa, Tatsuya Shishidou, Michael Weinert, and Kazuyuki Sakamoto*

Cite This: *Nano Lett.* 2023, 23, 7675−7682

Read Online

ACCESS | Metrics & More | Article Recommendations | Supporting Information

ABSTRACT: The interplay of spin−orbit coupling and crystal symmetry can generate spin-polarized bands in materials only a few atomic layers thick, potentially leading to unprecedented physical properties. In the case of bilayer materials with global inversion symmetry, locally broken inversion symmetry can generate degenerate spin-polarized bands, in which the spins in each layer are oppositely polarized. Here, we demonstrate that the hidden spins in a Tl bilayer crystal are revealed by growing it on Ag(111) of sizable lattice mismatch, together with the appearance of a remarkable phenomenon unique to centrosymmetric hidden-spin bilayer crystals: a novel band splitting in both spin and space. The key to success in observing this novel splitting is that the interaction at the interface has just the right strength: it does not destroy the original wave functions of the Tl bilayer but is strong enough to induce an energy separation.

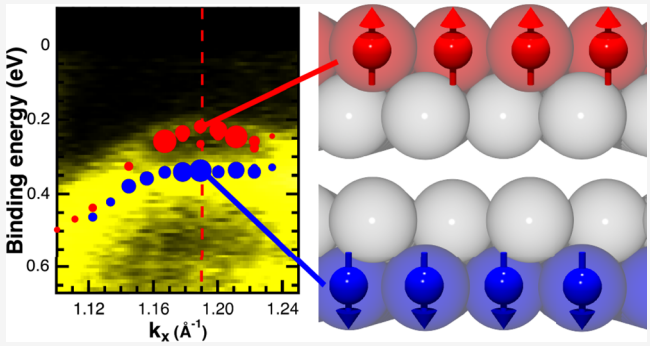

KEYWORDS: *bilayer material, hidden spin, superconductor, photoelectron spectroscopy, spintronics*

The decrease in dimension of a crystal from 3D bulk to 2D atomic layer materials (ALMs) with a thickness of one to a few atoms is often accompanied by the appearance of novel exotic physical properties. For example, ALMs with a thickness of one atom, such as graphene,[1−3] silicene, and germanene,[4] borophene[5] host Dirac Fermions, and an ALM two atoms thick, bilayer graphene, show superconductivity with a critical temperature (T_c) of up to 1.7 K.[6] The combination of superconductivity with spin-polarized bands − which arise from the so-called Rashba−Bychkov (or simply "Rashba") effect[7] and/or by the orbital angular momentum (OAM)[8−13] − may lead to further interesting physical properties and novel superconducting states;[14−16] a bilayer ALM superconductor formed from a heavy element with strong spin−orbit coupling (SOC) is a candidate of such an exotic superconductor. In the case of a centrosymmetric (globally symmetric) bilayer crystal, the individual layers have a locally broken inversion symmetry (Figure 1(a)). The global inversion guarantees the twofold spin degeneracy of the bands. The local inversion asymmetry can give rise to a staggered Rashba SOC in each layer.[17] However, in contrast to the normal Rashba effect, the overall twofold spin degeneracy of the bands is not lifted in this case, as shown in Figure 1(b). Similarly, Zeeman-type spins on each layer can also arise from the local inversion asymmetry, again with the spin hidden, as shown in Figure 1(c). Hidden spins were also predicted theoretically in centrosymmetric layered crystals,[17,18] and evidence of the hidden spin was reported experimentally[19−24] by considering, e.g., the limited detection depth of the measurement (mean free path of the photoelectron), which is longer than the thickness of a bilayer material.

The heavy element Tl is known to undergo a superconducting transition at approximately 2.4 K in its bulk phase.[25−32] Its predicted band structure[33−36] was expected to show a large spin−orbit splitting at the H point of the 3D Brillouin zone.[36] The band structure of a Tl single layer formed on Si or Ge has been reported to show semiconducting spin-polarized bands,[8−12,37−41] which means that they have no chance to become an atomic layer superconductor. A two-layer Tl film formed on Si(111) has been reported to become superconducting below 0.96 K,[42] but no spin-polarized states, or even no clear band structure, were observed. Furthermore,

Received: June 27, 2023
Revised: August 4, 2023
Published: August 14, 2023

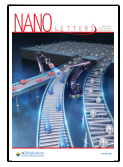

Downloaded via 87.227.14.227 on September 7, 2023 at 09:28:56 (UTC).
See https://pubs.acs.org/sharingguidelines for options on how to legitimately share published articles.

ACS Publications

© 2023 The Authors. Published by American Chemical Society

https://doi.org/10.1021/acs.nanolett.3c02387
Nano Lett. 2023, 23, 7675−7682

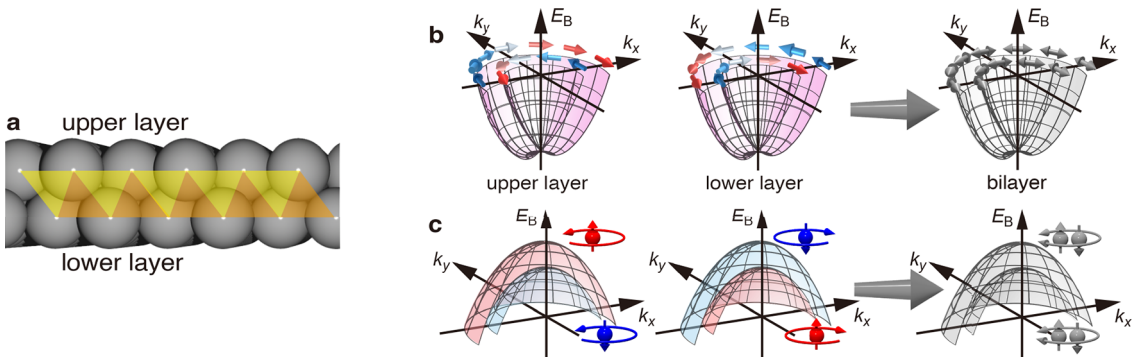

Figure 1. (a) Schematic illustration of the local inversion asymmetry of a centrosymmetric bilayer crystal, as indicated by triangles with different colors. (b and c) Illustration of bands with hidden (b) Rashba-type spin and (c) Zeeman-type spin. In (b), the direction of the spins is indicated by arrows. In (c), the arrows through the spheres indicate the direction of the spins, and the arrows of the arcs around them show the orbital motion of the electrons.

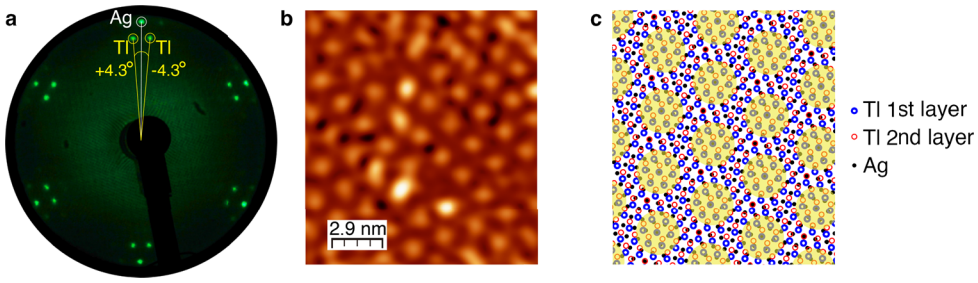

Figure 2. (a) LEED pattern of a Tl bilayer crystal grown on Ag(111) taken with a primary electron energy of 52 eV. (b) STM image of a Tl bilayer measured at a bias voltage of 1 V and a tunneling current of 1.2 nA. (c) Schematic illustration of the atomic structure of a Tl bilayer crystal formed on Ag(111). The first Tl layer means the outermost layer, and the second one is the layer adjacent to Ag. The yellow circles indicate the area centered where the second layer Tl atoms are located above the Ag atoms on the surface.

the same band as that of the Tl single layer formed on Si(111) was observed in this system, indicating that this system could be described as the addition of two Tl overlayers rather than an adsorbed bilayer crystal. The ideal freestanding Tl bilayer can host hidden spin polarization.[17] Although the bilayer is globally centrosymmetric (space group $P\bar{3}m1$), the Tl atoms in each layer have polar site symmetry C_{3v}, which allows local spin polarization to emerge. In particular, the Zeeman-type spin polarization (Figure 1(c)) is expected to appear in a Kramers doublet at the $\bar{K}$ point of the 2D Brillouin zone.

Here, we report our successful synthesis of the Tl bilayer crystal grown on Ag(111) and measurements of its band structure, spin polarization, and electrical transport properties. Around the $\bar{K}$ point, Tl states are found in the Ag band gaps. There, the interactions with the substrate are limited, serving only to slightly lift the energy degeneracy of the bilayer-inherent hidden spin states and enabling us to observe a remarkable splitting phenomenon involving both spin and space. This splitting differs from the standard Rashba or Zeeman-type splitting in non-centrosymmetric crystals, where essentially only the spin degrees of freedom are involved in lifting the degenerate bands. This splitting may have a significant impact on transport properties such as superconductivity, which the Tl bilayer crystal was found to exhibit at 0.9 K in this study.

High-quality bilayer Tl crystals were formed on Ag(111). The sample quality was confirmed by the observations of sharp spots with low background intensity by low-energy electron diffraction (LEED). The spin-integrated and spin-polarized band structures were obtained experimentally by high-resolution angle-resolved photoelectron spectroscopy (ARPES) and spin-resolved ARPES (SARPES) and theoretically by density functional theory (DFT) calculations. Both ARPES and SARPES measurements were conducted between 30 and 100 K. Scanning tunneling microscopy (STM) measurements were performed at 4.2 K. The electrical transport measurements were performed using a sub-Kelvin micro four-point probe.[43] All experiments were conducted in ultrahigh vacuum (UHV) chambers under a base pressure of $<1 \times 10^{-8}$ Pa. Details of the sample preparation and details of the experimental setup and theoretical calculations are described in the Supporting Information.

A Tl bilayer formed on Ag(111) has been reported to have a lattice constant close to that of bulk Tl, with the interaction between the Tl and Ag atoms at the interface being weak.[44,45] The LEED pattern of a Tl bilayer crystal formed on Ag(111) in this work is shown in Figure 2(a). Six pairs of three spots with high intensity are clearly observed together with weaker intensity spots. By comparing the LEED patterns of before and after Tl deposition, we attribute the outer one of the three spots to originate from Ag(111) and the inner two to originate from the Tl bilayer crystal. The directions of the two spots from Tl are rotated ±4.3° from the unit vector of Ag(111), indicating the presence of two Tl bilayer domains.

The ratio of the distance between the LEED spots originating from a single Tl bilayer domain and from the Ag substrate is approximately 1:1.2. This ratio indicates the in-plane nearest-neighbor spacing of Tl atoms to be approximately 3.45 Å, a value close to that in bulk Tl. Both the in-plane nearest-neighbor distance and the rotation angle are in

https://doi.org/10.1021/acs.nanolett.3c02387
Nano Lett. 2023, 23, 7675−7682

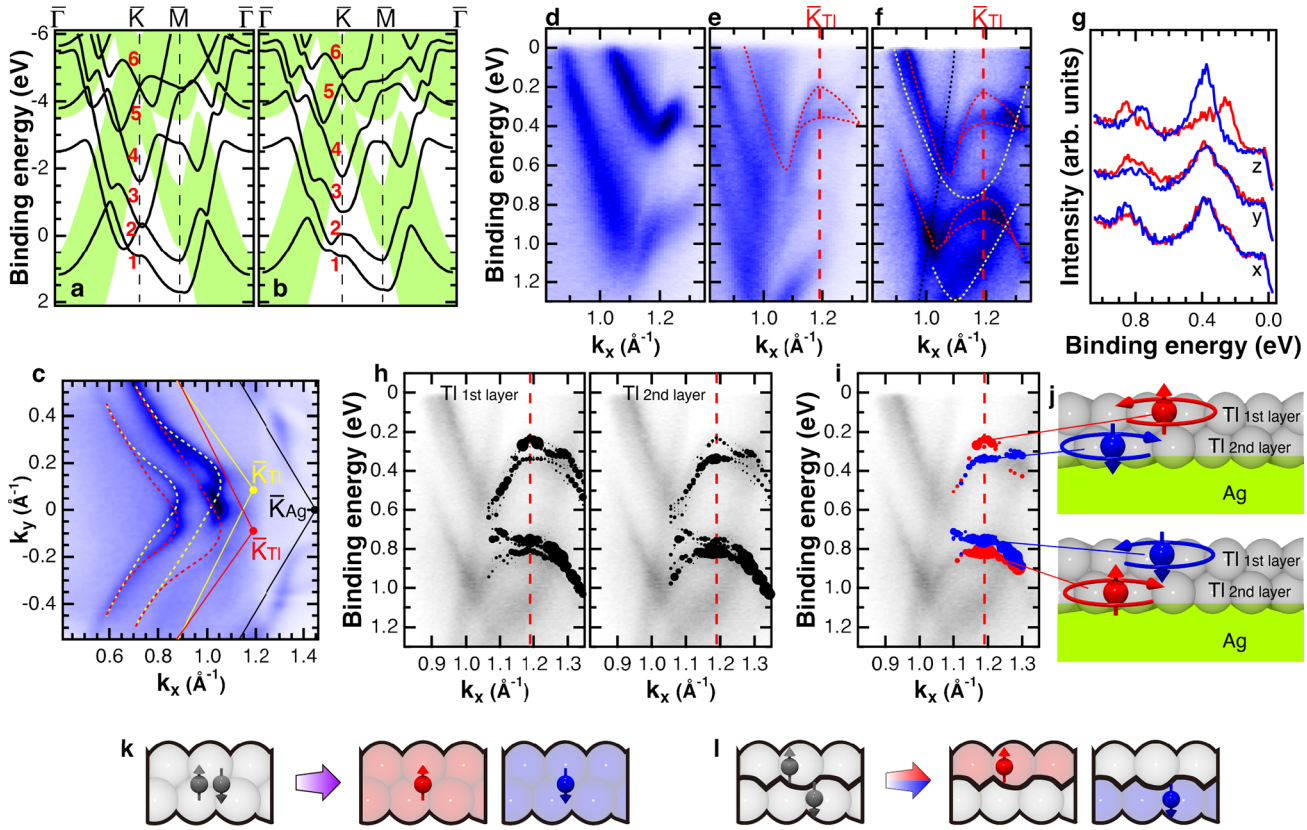

Figure 3. (a and b) Theoretically obtained band structures of a freestanding Tl bilayer crystal (a) without SOC and (b) with SOC. The green shaded areas indicate where Ag bulk states are expected to appear. (c) Fermi surface of Tl bilayer crystals grown on Ag(111) measured at $h\nu$ = 40 eV. The black solid line represents the Brillouin zone of the Ag(111) surface, and the red and yellow solid lines represent the Brillouin zones of the two domains of Tl. $\bar{K}_{Ag}$ and $\bar{K}_{Tl}$ are the $\bar{K}$ points of the Brillouin zones of Ag(111) and Tl bilayer crystals. (d) Band dispersion obtained with $h\nu$ = 40 eV along k_x at k_y = 0 Å^{-1}. (e and f) Band along k_x at k_y = −0.09 Å^{-1} measured at $h\nu$ = (e) 40 and (f) 21.2 eV. The red (yellow) dotted lines are guides for the bands derived from the Tl bilayer of the red (yellow) Brillouin zone, and the black dotted line guides the band originating from Ag. (g) Spin-resolved EDC curves at the $\bar{K}_{Tl}$ point. Red (blue) data in (g) indicate spins in the positive (negative) direction of each axis. The black circles in (h) show the theoretically obtained band structures of a Tl bilayer crystal grown on Ag(111), and their size shows the weight of orbitals from Tl atoms of the first layer and those from Tl of the second layer in each panel. (i) Theoretically obtained spin polarization along the z direction. (j) Schematic illustration of layer-dependent spin polarization. (k and l) Band splitting of a standard Rashba effect and that of a staggered Rashba SOC system. In (c−f, h, and i), the shading from light to dark indicates the relative measured intensities.

agreement with those reported in ref 45. (The slightly longer Tl−Tl distance obtained in the present study compared to that in ref 45 might result from the difference in Tl bilayer formation; i.e., the sample was prepared in ultrahigh vacuum conditions in the present study, while it was formed in an electrolyte in ref 45.) The lattice parameters of the Tl bilayer crystal on Ag(111) were also confirmed by STM. Figure 2(b) shows the STM image of the Moiré pattern induced by the difference in Tl−Tl and Ag−Ag distances and by the rotation angle of the Tl bilayer. The distance between two protrusions in STM is approximately 15 Å (Figure 2(b)), a value consistent with the distance between two Tl atoms with the same environment, e.g., the two second layer Tl atoms situated on top of Ag that are highlighted by yellow circles in the schematic illustration of Figure 2(c). This agreement between Figure 2(b) and (c) also confirms the lattice parameters of the Tl bilayer crystal on Ag(111). Moreover, the threefold symmetry observed in LEED and STM indicates that the atomic structure of the epitaxially grown Tl bilayer crystal on Ag(111) is basically identical to that of an ideal freestanding Tl bilayer whose atomic structure belongs to the space group $P\bar{3}m1$.

The band dispersions of a freestanding Tl bilayer crystal calculated without and with SOC are shown in Figure 3(a) and (b), respectively. Of the six bands labeled 1−6, the two labeled 2 and 3 and those labeled 5 and 6 are degenerated at the $\bar{K}$ point in (a). SOC lifts these degeneracies but otherwise does not change the dispersions of bands much. As shown in Table 1, the components of the wave functions of the three bands located close to the Fermi level at $\bar{K}$ (the bands labeled 1, 2, and 3) indicate that the p electrons of both the upper and lower Tl layers have a large contribution to each of these three bands and that when the p_x and p_y components of the upper layer Tl induce the OAM pointing the $+z$ ($-z$) direction, those of the lower layer induce the OAM pointing in the $-z$ ($+z$) direction simultaneously. Here, x and y are the two orthogonal axes parallel to the atomic layer, and z is the axis along the direction perpendicular to the atomic layer. This OAM direction at $\bar{K}$ agrees well with that predicted for ALMs with atomic structure belonging to the space group $P\bar{3}m1$.[8−12] Since the spin tends to become parallel to the OAM,[9,13] the presence of OAMs pointing in opposite directions in a single band at different atomic sites indicates that the spins pointing along the z direction at $\bar{K}$ are hidden in a freestanding Tl bilayer crystal, as in the illustration in Figure 1(c). A way to reveal these

https://doi.org/10.1021/acs.nanolett.3c02387
Nano Lett. 2023, 23, 7675−7682

Table 1. Components of the Wave Functions of the Bands Labeled 1, 2, and 3 Obtained (a) without SOC in Figure 3(a) and (b) with SOC in Figure 3(b)[a]

a

band	spin	lower layer				upper layer			
		Y_0^0	Y_1^{-1}	Y_1^0	Y_1^1	Y_0^0	Y_1^{-1}	Y_1^0	Y_1^1
1			**0.71*w***						**0.71**
2,3		0.40		0.41			**-0.82*w***		
					0.82*w**	-0.40		0.41	

b

band	spin	lower layer				upper layer			
		Y_0^0	Y_1^{-1}	Y_1^0	Y_1^1	Y_0^0	Y_1^{-1}	Y_1^0	Y_1^1
1	up		**0.85**						0.46*w*
	down	-0.07		-0.24			0.10*w*		
	up				-0.10	0.07*w*		-0.24*w*	
	down		0.46						**0.85*w***
2	up	-0.02	-0.23						
	down				**0.83**	-0.39*w*		0.32*w*	
	up	-0.39		-0.32			**0.83w**		
	down					0.02*w*		-0.23*w*	
3	up				**0.77**	-0.39*w*		0.45*w*	
	down		0.23						
	up								-0.23
	down	-0.38*w*		-0.45*w*			**0.77**		

[a]The largest contribution is indicated in bold ($w = \exp(i2\pi/3)$).

hidden spins is to break the space inversion symmetry along the z direction slightly, which can be done by growing the Tl bilayer on a solid surface. Owing to the large lattice mismatch with Ag(111) and the large energy gap of the projected Ag bulk states (the shaded areas in Figure 3(a) and (b)), the Tl states can maintain their original Tl bilayer wave functions around $\bar{K}$ and, as presented below, show a novel splitting with respect to both spin and spatial distribution.

The Fermi surface of the Tl bilayer crystal grown on Ag obtained by ARPES with a photon energy ($h\nu$) of 40 eV is shown in Figure 3(c). The red and yellow hexagons are the boundaries of the first Brillouin zones of the two Tl bilayer domains, and the black hexagon shows that of Ag(111). The subscripts Tl and Ag of $\bar{K}$ indicate to which Brillouin zone the symmetry point corresponds. Four Fermi surfaces, indicated by dashed lines, are observed inside the first Brillouin zones of the Tl bilayer crystals in Figure 3(c). These four Fermi surfaces are observed at the same (k_x,k_y) in measurements performed at different $h\nu$ (Supporting Information, Figure S4), meaning that these states do not have a k_z dependence and thus originate from the Tl bilayer crystal. Figure 3(d) shows the band dispersion measured with $h\nu$ = 40 eV along $\bar{\Gamma} - \bar{K}_{Ag}$ (k_y = 0 Å^{-1}), i.e., the k line along which the two Tl Brillouin zones are mirror images and thus the bands from the two Tl bilayer domains show identical dispersion. As shown in the figure, there are two bands crossing the Fermi level (E_F) at approximately k_x = 0.875 and 1.05 Å^{-1}, indicating the number of metallic bands delivered from a single Tl bilayer domain to be two. Thus, the observation of four metallic Fermi surfaces in Figure 3(c) arises from the presence of two domains.

Figure 3(e) shows the band dispersion measured with $h\nu$ = 40 eV along the k_x direction at k_y = −0.09 Å^{-1}. Note that $\bar{K}_{Tl}$, the $\bar{K}$ point of the Brillouin zone of the Tl bilayer crystal, is located at (k_x = 1.20 Å^{-1}, k_y = ±0.09 Å^{-1}) given the fact that the domains are rotated ±4.3° from that of Ag(111). The dispersion of the band, guided by the red dotted lines in Figure 3(e), shows good correspondence with that of the band labeled 2 in Figure 3(b) along $\bar{\Gamma} - \bar{K}$: both the experimentally obtained band of a Tl bilayer on Ag(111) and the theoretically obtained one of a freestanding Tl bilayer show downward dispersions from $\bar{\Gamma}$, cross the Fermi level, turn upward, and show convex upward structures around $\bar{K}$ ($\bar{K}_{Tl}$). However, the critical difference from the theoretical band is that the band of the Tl bilayer on Ag(111) splits into two around the $\bar{K}_{Tl}$ point. In order to obtain more detailed information about the origin of the observed split band, we have measured the band dispersion along the k_x direction at k_y = −0.09 Å^{-1} with $h\nu$ = 21.2 eV (Figure 3(f)). There are four bands derived from the two Tl bilayer domains (red and yellow dotted lines) and a band originating from Ag (black dotted line). The red (yellow) dotted lines indicate bands from the red (yellow) Brillouin zone in Figure 3(c), meaning that the red dotted bands cross the $\bar{K}_{Tl}$ point while yellow ones are off from this symmetry

https://doi.org/10.1021/acs.nanolett.3c02387
Nano Lett. 2023, 23, 7675−7682

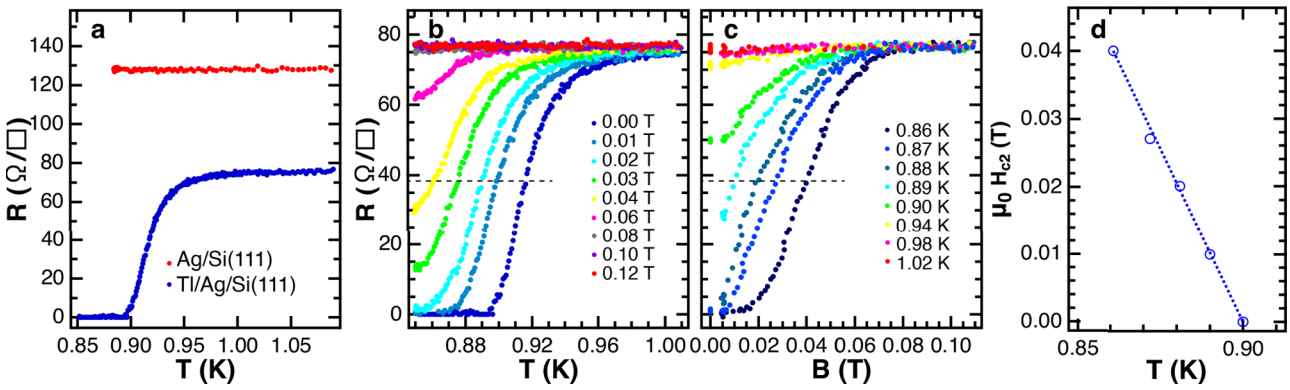

Figure 4. (a) Temperature dependence of sheet resistance at zero magnetic field. The red and blue dots show the sheet resistance of a Ag film grown on Si(111) and the Tl bilayer crystal grown on it. (b) Temperature-dependent sheet resistance under different magnetic fields perpendicular to the plane. (c) Magnetic field-dependent sheet resistance at different temperatures. (d) Temperature dependence of the upper critical field. The broken line in (d) is the fitting result by the GL theory.

point. Therefore, we conclude that both of the metallic bands of a Tl bilayer crystal are split at $\bar{K}_{Tl}$.

The spin-resolved energy distribution curves (EDCs) at $\bar{K}_{Tl}$, obtained by SARPES, are displayed in Figure 3(g). These results show that the splittings of the two bands observed in Figure 3(f) at $\bar{K}_{Tl}$ are spin splittings and that the spins point along the z direction, as expected from the OAM that arises from the C_3 symmetry of $\bar{K}_{Tl}$ and confirmed by theoretical calculations as shown in Figure 3(i). Given that the two spin-split bands correspond to the bands labeled 1 and 2 in Figure 3(a) and (b), and by considering the p orbital components of the eigenvectors of these two bands, the spin splitting observed at $\bar{K}_{Tl}$ in Figure 3(f) is induced by the small perturbation from the Ag substrate that makes the two Tl layers slightly inequivalent, thereby revealing the hidden spins. For a freestanding Tl bilayer, symmetry dictates that the bands labeled 1 and 2 are degenerate at $\bar{K}_{Tl}$ with the spins in the two layers pointing oppositely along $\pm z$. In contrast, for the broken symmetry case of Tl on a Ag(111) substrate, there should be a small difference in the relative weight of the Tl orbitals of the first and second layers in each split band. (The first layer is the outermost layer, and the second one is the interface layer, as denoted in Figure 2(c) and 3(j).)

The calculated contributions of the Tl orbitals of the first and second layers are shown in Figure 3(h), where the size of the circles corresponds to the weight of orbitals. There is a clear layer-dependent orbital contribution to the spin split band; i.e., the orbitals of Tl from the first layer mainly contribute to the spin split band located at binding energies (E_B) ~ 0.24 and 0.75 eV at $\bar{K}_{Tl}$, and those from the second layer, to the spin split bands at E_B ~ 0.38 and 0.82 eV. By combining this layer-dependent contribution and the orientation of the spins of the split band, we conclude that the inducement of a small perturbation by the Ag substrate has revealed the hidden spins of a Tl bilayer crystal by splitting the bands in both spin and space as shown in Figure 3(j). This band splitting in both spin and space is fundamentally different from a standard Rashba splitting, where the band splits only in spin, and is peculiar to a bilayer crystal with staggered Rashba SOC as shown in Figure 3(k) and (l). Furthermore, this way of exposing hidden spins provides a deeper understanding and new insights into the spin physics of bilayer ALMs formed on solid surfaces and will also open a pathway for the application uses of such materials.

It is further interesting to examine the transport property of a Tl bilayer crystal on Ag(111). Figure 4(a) shows the temperature-dependent sheet resistivity of a 10 ML thick Ag(111) film grown on Si(111) and that of the Tl bilayer crystal grown on it. The resistivity of the Tl bilayer is 77 Ω/□ at 1.1 K, a value lower than that of the Ag(111) film (~128 Ω/□). This lower resistivity indicates the Tl bilayer to be metallic and agrees well with the observation of metallic bands in ARPES. At lower temperature, the Tl bilayer shows a drop in sheet resistance to 0 Ω/□ at approximately 0.9 K. The midpoint of the drop, ~38.5 Ω/□, gives the T_c to be ~0.92 K. This T_c is lower than that of bulk Tl, 2.4 K, probably due to the proximity effect of the metallic Ag substrate and/or from the 2D dimensionality of the Tl bilayer crystal that lowers the Debye temperature and thus the T_c. The gradual drop in resistance is a phenomenon typically observed in 2D superconductors, as shown in, e.g., refs 46 and 47.

When applying a magnetic field perpendicular to the Tl layer, the temperature where the sheet resistance drops becomes lower, and the superconductivity is destroyed at 0.08 T (Figure 4(b)). The magnetoresistance at different temperatures is also displayed in Figure 4(c). In Figure 4(d), we show the temperature dependence of the upper critical field, $\mu_0 H_{c2}(T)$. ($\mu_0 H_{c2}(T)$ is defined as the point at which the sheet resistance is half of the normal state one, ~38Ω/□, and is obtained from Figure 4(b) and (c).) The linear relation of $\mu_0 H_{c2}(T)$ with temperature is what is expected within the framework of Ginzburg−Landau (GL) theory, $\mu_0 H_{c2}(T) = \phi_0/2\pi\xi_{GL}(T)^{1/2} = \phi_0 \times (1 - T/T_c)/2\pi\xi_{GL}(0)^{1/2}$; the broken line in Figure 4(d) is a fitting of the experimental data and gives the coherence length at 0 K, $\xi_{GL}(0)$, of 220 Å. This value is much longer than the thickness of the Tl bilayer crystal, indicating that the Tl bilayer crystal is a 2D superconductor. Since a Tl bilayer crystal is a 2D superconductor with spin-polarized bands, this system may show further interesting spin-related physical properties.

In conclusion, we succeeded in revealing the hidden spin-polarized bands of a Tl bilayer crystal by applying a small perturbation via a substrate to the wave function of Tl atoms of one of the two layers. This small perturbation is weak and does not modify the band structure significantly from that of a freestanding Tl bilayer crystal but is strong enough to split the band in both spin and space. In this respect, the present results not only show a novel band splitting peculiar to bilayer crystal

https://doi.org/10.1021/acs.nanolett.3c02387
Nano Lett. 2023, 23, 7675−7682

with staggered Rashba SOC but also exceed the previous studies observing the hidden spins in the sense of practical use: Previously, the oppositely oriented spins were still degenerate so that the bands with these hidden spins behave like nonpolarized bands; i.e., the spins with opposite polarization move together like a normal electric current in response to a potential difference across the sample. On the other hand, in the present work, the lifting of the degeneracy leads to the bands becoming spin polarized and the possibility of spin-polarized currents, a necessary condition to realize spintronics devices. Furthermore, the Tl bilayer crystal becomes superconducting below 0.9 K and therefore has the possibility of showing spin-related novel superconducting states. Extensions of the present approach of exposing hidden spin-polarized bands to other 2D superconductors and producing superconducting quantum spintronics devices are exciting directions for future work.

■ ASSOCIATED CONTENT

Supporting Information

The Supporting Information is available free of charge at https://pubs.acs.org/doi/10.1021/acs.nanolett.3c02387.

Details of sample preparation, details of photoemission and STM, confirmation of the Tl layer thickness, fast Fourier transform and autocorrelation function of STM data, photon energy-dependent Fermi surface and band dispersion of the Tl bilayer crystal grown on Ag, symmetry of the Fermi surface, split at the $\bar{K}_{Tl}$ points of the two Tl domains, band structure of the Tl bilayer crystal grown on Ag/Si(111), details of the DFT calculations, examination of different interface structures, comparison of the band dispersion obtained by tight-binding calculation and DFT, layer-resolved OAM and induced spin moments and spin density distribution. (PDF)

■ AUTHOR INFORMATION

Corresponding Author

Kazuyuki Sakamoto − *Department of Applied Physics and Spintronics Research Network Division, Institute for Open and Transdisciplinary Research Initiatives, Osaka University, Osaka 565-0871, Japan; Center for Spintronics Research Network, Osaka University, Osaka 560-8531, Japan;* orcid.org/0000-0001-9507-6435; Email: kazuyuki_sakamoto@ap.eng.osaka-u.ac.jp

Authors

Takahiro Kobayashi − *Department of Material and Life Science, Osaka University, Osaka 565-0871, Japan*

Yuichiro Toichi − *Department of Applied Physics, Osaka University, Osaka 565-0871, Japan;* orcid.org/0000-0002-1883-0817

Koichiro Yaji − *Research Center for Advanced Measurement and Characterization, National Institute for Materials Science, Ibaraki 305-0047, Japan*

Yoshitaka Nakata − *Department of Materials Science, Chiba University, Chiba 263-8522, Japan*

Yuchi Yaoita − *Department of Materials Science, Chiba University, Chiba 263-8522, Japan*

Mutsuki Iwaoka − *Department of Materials Science, Chiba University, Chiba 263-8522, Japan*

Mariko Koga − *Department of Materials Science, Chiba University, Chiba 263-8522, Japan*

Yituo Zhang − *Department of Materials Science, Chiba University, Chiba 263-8522, Japan*

Jun Fujii − *Istituto Officina dei Materiali, Consiglio Nazionale delle Ricerche (CNR-IOM), I-34149 Trieste, Italy*

Shimpei Ono − *Central Research institute of Electric Power Industry, Yokosuka 240-0196, Japan*

Yasmine Sassa − *Department of Physics, Chalmers University of Technology, Göteborg 412 96, Sweden;* orcid.org/0000-0003-1416-5642

Yasuo Yoshida − *Institute for Solid State Physics, The University of Tokyo, Chiba 277-8581, Japan;* Present Address: (Y.Y.) Present address: Department of Physics, Kanazawa University, Kanazawa, Ishikawa 920-1192, Japan

Yukio Hasegawa − *Institute for Solid State Physics, The University of Tokyo, Chiba 277-8581, Japan;* orcid.org/0000-0002-6674-4745

Fumio Komori − *Institute for Solid State Physics, The University of Tokyo, Chiba 277-8581, Japan;* orcid.org/0000-0002-6405-4177

Shik Shin − *Institute for Solid State Physics, The University of Tokyo, Chiba 277-8581, Japan*

Satoru Ichinokura − *Department of Physics, The University of Tokyo, Tokyo 113-0033, Japan;* Present Address: (S.I.) Department of Physics, Tokyo Institute of Technology, Tokyo 152-8551, Japan.; orcid.org/0000-0002-7968-4016

Ryota Akiyama − *Department of Physics, The University of Tokyo, Tokyo 113-0033, Japan;* orcid.org/0000-0003-3875-9509

Shuji Hasegawa − *Department of Physics, The University of Tokyo, Tokyo 113-0033, Japan*

Tatsuya Shishidou − *Department of Physics, University of Wisconsin, Milwaukee, Wisconsin 53201, United States*

Michael Weinert − *Department of Physics, University of Wisconsin, Milwaukee, Wisconsin 53201, United States;* orcid.org/0000-0002-2263-2960

Complete contact information is available at: https://pubs.acs.org/10.1021/acs.nanolett.3c02387

Author Contributions

T.K., Y.T., K.Y., Y.N., Y.Ya., M.I, J.F., S.O., Y.S., F.K., S.S., and K.S. carried out the photoemission measurements; Y.Z., Y.Yo., and Y.H. performed the STM measurements; M.I, M.K., S.I., R.A., and S.H. carried out the transport measurements; Y.T., T.S., and M.W performed the theoretical calculations. K.S. initiated the research, designed the project, and wrote the manuscript with the help of all the authors. All the authors discussed the results and commented on the manuscript.

Notes

The authors declare no competing financial interest.

■ ACKNOWLEDGMENTS

This research was supported by JSPS KAKENHI Grants No. JP22H01957, No. JP20H02616, No. JP19H02592, No. JP20H05621, No. JP20H00342, No. JP16H02108, No. JP21H05016, No. JP18K03484, and No. JP18K18732. T.S. and M.W. were supported by the U.S. Department of Energy, Office of Basic Energy Sciences, Division of Materials Sciences and Engineering, under Award No. DE-SC0017632. Y.S. was

supported by the Swedish Research Council (VR) through a Starting Grant (Dnr. 2017-05078), Area of Advances-Material Sciences from Chalmers University of Technology, and Wallenberg Young Fellow through the grant KAW 2021.0150. This work has been partly performed in the framework of the nanoscience foundry and fine analysis (NFFA-MIUR Italy Progetti Internazionali) facility.

■ ABBREVIATIONS

ALM	atomic layer material
T_c	critical temperature
OAM	orbital angular momentum
SOC	spin−orbit coupling
ARPES	angle-resolved photoelectron spectroscopy
STM	scanning tunneling microscopy
SARPES	spin-resolved ARPES
DFT	density-functional theory
UHV	ultrahigh vacuum
EDC	energy distribution curves
E_B	binding energy

■ REFERENCES

(1) Novoselov, K. S.; Geim, A. K.; Morozov, S. V.; Jiang, D.; Katsnelson, M. I.; Grigorieva, I. V.; Dubonos, S. V.; Firsov, A. A. Two-dimensional gas of massless Dirac fermions in graphene. *Nature* **2005**, *438*, 197−200.

(2) Zhang, Y.; Tan, Y.-W.; Stormer, H. L.; Kim, P. Experimental observation of the quantum Hall effect and Berry's phase in graphene. *Nature* **2005**, *438*, 201−204.

(3) Wallace, P. R. The Band Theory of Graphite. *Phys. Rev.* **1947**, *71*, 622−634.

(4) Cahangirov, S.; Topsakal, M.; Aktürk, E.; Sahin, H.; Ciraci, S. Two- and one-dimensional honeycomb structures of silicon and germanium. *Phys. Rev. Lett.* **2009**, *102*, 236804.

(5) Feng, B.; Sugino, O.; Liu, R.-Y.; Zhang, J.; Yukawa, R.; Kawamura, M.; Iimori, T.; Kim, H.; Hasegawa, Y.; Li, H.; Chen, L.; Wu, K.; Kumigashira, H.; Komori, F.; Chiang, T. -Ch.; Meng, S.; Matsuda, I. Dirac fermions in borophene. *Phys. Rev. Lett.* **2017**, *118*, 096401.

(6) Cao, Y.; Fatemi, V.; Fang, S.; Watanabe, K.; Taniguchi, T.; Kaxiras, E.; Jarillo-Herrero, P. Unconventional superconductivity in magic-angle graphene superlattices. *Nature* **2018**, *556*, 43−50.

(7) Bychkov, Y. A.; Rashba, E. I. Properties of a 2D electron gas with lifted spectral degeneracy. *JETP Lett.* **1984**, *39*, 78−81.

(8) Oguchi, T.; Shishidou, T. The surface Rashba effect: a *k·p* perturbation approach. *J. Phys.: Condens. Matter* **2009**, *21*, 092001.

(9) Sakamoto, K.; Oda, T.; Kimura, A.; Miyamoto, K.; Tsujikawa, M.; Imai, A.; Ueno, N.; Namatame, H.; Taniguchi, M.; Eriksson, P. E. J.; Uhrberg, R. I. G. Abrupt rotation of the Rashba spin to the direction perpendicular to the surface. *Phys. Rev. Lett.* **2009**, *102*, 096805.

(10) Sakamoto, K.; Kim, T.-H.; Kuzumaki, T.; Müller, B.; Yamamoto, Y.; Ohtaka, M.; Osiecki, J. R.; Miyamoto, K.; Takeichi, Y.; Harasawa, A.; Stolwijk, S. D.; Schmidt, A. B.; Fujii, J.; Uhrberg, R. I. G.; Donath, M.; Yeom, H. W.; Oda, T. Valley spin polarization by using the extraordinary Rashba effect on silicon. *Nat. Commun.* **2013**, *4*, 2073.

(11) Stolwijk, S. D.; Schmidt, A. B.; Donath, M.; Sakamoto, K.; Krüger, P. Rotating spin and giant splitting: Unoccupied surface electronic structure of Tl/Si(111). *Phys. Rev. Lett.* **2013**, *111*, 176402.

(12) Stolwijk, S. D.; Schmidt, A. B.; Sakamoto, K.; Krüger, P.; Donath, M. Valley spin polarization of Tl/Si(111). *Phys. Rev. Mater.* **2017**, *1*, 064604.

(13) Kobayashi, T.; Nakata, Y.; Yaji, K.; Shishidou, T.; Agterberg, D.; Yoshizawa, S.; Komori, F.; Shin, S.; Weinert, M.; Uchihashi, T.; Sakamoto, K. Orbital angular momentum induced spin polarization of 2D metallic bands. *Phys. Rev. Lett.* **2020**, *125*, 176401.

(14) Sau, J. D.; Lutchyn, R. M.; Tewari, S.; Das Sarma, S. Generic new platform for topological quantum computation using semiconductor heterostructures. *Phys. Rev. Lett.* **2010**, *104*, 040502.

(15) Smidman, M.; Salamon, M. B.; Yuan, H. Q.; Agterberg, D. F. Superconductivity and spin-orbit coupling in non-centrosymmetric materials: a review. *Rep. Prog. Phys.* **2017**, *80*, 036501.

(16) Masutomi, R.; Okamoto, T.; Yanase, Y. Unconventional superconducting phases in multilayer films with layer-dependent Rashba spin-orbit interactions. *Phys. Rev. B* **2020**, *101*, 184502.

(17) Zhang, X.; Liu, Q.; Luo, J.-W.; Freeman, A. J.; Zunger, A. Hidden spin polarization in inversion-symmetric bulk crystals. *Nat. Phys.* **2014**, *10*, 387−393.

(18) Liu, Q.; Zhang, X.; Jin, H.; Lam, K.; Im, J.; Freeman, A. J.; Zunger, A. Search and design of nonmagnetic centrosymmetric layered crystals with large local spin polarization. *Phys. Rev. B* **2015**, *91*, 235204.

(19) Riley, J. M.; Mazzola, F.; Dendzik, M.; Michiardi, M.; Takayama, T.; Bawden, L.; Granerød, C.; Leandersson, M.; Balasubramanian, T.; Hoesch, M.; Kim, T. K.; Takagi, H.; Meevasana, W.; Hofmann, P.; Bahramy, M. S.; Wells, J. W.; King, P. D. C. Direct observation of spin-polarized bulk bands in an inversion-symmetric semiconductor. *Nat. Phys.* **2014**, *10*, 835−839.

(20) Razzoli, E.; Jaouen, T.; Mottas, M.-L.; Hildebrand, B.; Monney, G.; Pisoni, A.; Muff, S.; Fanciulli, M.; Plumb, N. C.; Rogalev, V. A.; Strocov, V. N.; Mesot, J.; Shi, M.; Dil, J. H.; Beck, H.; Aebi, P. Selective probing of hidden spin-polarized states in inversion-symmetric bulk MoS_2. *Phys. Rev. Lett.* **2017**, *118*, 086402.

(21) Yao, W.; Wang, E.; Huang, H.; Deng, K.; Yan, M.; Zhang, K.; Miyamoto, K.; Okuda, T.; Li, L.; Wang, Y.; Gao, H.; Liu, C.; Duan, W.; Zhou, S. Direct observation of spin-layer locking by local Rashba effect in monolayer semiconducting $PtSe_2$ film. *Nat. Commun.* **2017**, *8*, 14216.

(22) Wu, S.-L.; Sumida, K.; Miyamoto, K.; Taguchi, K.; Yoshikawa, T.; Kimura, A.; Ueda, Y.; Arita, M.; Nagao, M.; Watauchi, S.; Tanaka, I.; Okuda, T. Direct evidence of hidden local spin polarization in a centrosymmetric superconductor $LaO_{0.55}F_{0.45}BiS_2$. *Nat. Commun.* **2017**, *8*, 1919.

(23) Gatti, G.; Gosálbez-Martínez, D.; Roth, S.; Fanciulli, M.; Zacchigna, M.; Kalläne, M.; Rossnagel, K.; Jozwiak, C.; Bostwick, A.; Rotenberg, E.; Magrez, A.; Berger, H.; Vobornik, I.; Fujii, J.; Yazyev, O. V.; Grioni, M.; Crepaldi, A. Hidden bulk and surface effects in the spin polarization of the nodal-line semimetal ZrSiTe. *Commun. Phys.* **2021**, *4*, 54.

(24) Zhang, K.; Zhao, S.; Hao, Z.; Kumar, S.; Schwier, E. F.; Zhang, Y.; Sun, H.; Wang, Y.; Hao, Y.; Ma, X.; Liu, C.; Wang, L.; Wang, X.; Miyamoto, K.; Okuda, T.; Liu, C.; Mei, J.; Shimada, K.; Chen, C.; Liu, Q. Observation of spin-momentum-layer locking in a centrosymmetric crystal. *Phys. Rev. Lett.* **2021**, *127*, 126402.

(25) Keesom, W. H.; Kok, J. A. Measurements of the specific heat of thallium at liquid helium temperatures. *Physica* **1934**, *1*, 175−181.

(26) Keesom, W. H.; Kok, J. A. Measurements of the latent heat of thallium connected with the transition, in a constant external magnetic field, from the supraconductive to the non-supraconductive state. *Physica* **1934**, *1*, 503−512.

(27) Daunt, J. G.; Horseman, A.; Mendelssohn, K. Thermodynamical properties of some supraconductors. *Philos. Mag.* **1939**, *27*, 754−764.

(28) Misener, A. D. The specific heat of superconducting mercury, indium and thallium. *Proc. R. Soc. London A* **1940**, *174*, 262−272.

(29) Maxwell, E.; Lutes, O. S. Threshold field properties of some superconductors. *Phys. Rev.* **1954**, *95*, 333−338.

(30) van der Hoeven Jr, B. J. C.; Keesom, P. H. Specific heat of mercury and thallium between 0.35 and 4.2 K. *Phys. Rev.* **1964**, *135*, A631.

(31) Magome, T.; Imamura, T.; Ohtsuka, M. Effect of fluctuations on the resistive superconducting transition in thallium film. *J. Phys. Soc. Jpn.* **1973**, *35*, 1555.

https://doi.org/10.1021/acs.nanolett.3c02387
Nano Lett. 2023, 23, 7675−7682

(32) Imamura, T.; Okamoto, K.; Saito, M.; Ohtsuka, M. Fluctuation-induced conductivity above the superconducting transition temperature in thallium films. *J. Phys. Soc. Jpn.* **1976**, *40*, 1256−1262.
(33) Soven, P. Relativistic band structure and Fermi surface of thallium. I. *Phys. Rev.* **1965**, *137*, A1706−A1717.
(34) Ament, M. A. E. A.; de Vroomen, A. R. Electronic structure and optical properties of thallium. *J. Phys. F: Met. Phys.* **1977**, *7*, 97−104.
(35) Holtham, P. M.; Jan, J.-P.; Skriver, H. L. Band structure of thallium by the LMTO method. *J. Phys. F: Met. Phys.* **1977**, *7*, 635−646.
(36) Heid, R.; Bohnen, K.-P.; Sklyadneva, I. Y.; Chulkov, E. V. Effect of spin-orbit coupling on the electron-phonon interaction of the superconductors Pb and Tl. *Phys. Rev. B* **2010**, *81*, 174527.
(37) Eriksson, P. E. J.; Sakamoto, K.; Uhrberg, R. I. G. Electronic structure of the thallium-induced 2 × 1 reconstruction on Si(001). *Phys. Rev. B* **2010**, *81*, 205422.
(38) Ohtsubo, Y.; Hatta, S.; Okuyama, H.; Aruga, T. A metallic surface state with uniaxial spin polarization on Tl/Ge(111)-(1 × 1). *J. Phys.: Condens. Matter* **2012**, *24*, 092001.
(39) Stolwijk, S. D.; Sakamoto, K.; Schmidt, A. B.; Krüger, P.; Donath, M. Thin line of a Rashba-type spin texture: Unoccupied surface resonance of Tl/Si(111) along. *Phys. Rev. B* **2014**, *90*, 161109.
(40) Stolwijk, S. D.; Sakamoto, K.; Schmidt, A. B.; Krüger, P.; Donath, M. Spin texture with a twist in momentum space for Tl/Si(111). *Phys. Rev. B* **2015**, *91*, 245420.
(41) Annese, E.; Kuzumaki, T.; Müller, B.; Yamamoto, Y.; Nakano, H.; Kato, H.; Araki, A.; Ohtaka, M.; Aoki, T.; Ishikawa, H.; Hayashida, T.; Osiecki, J. R.; Miyamoto, K.; Takeichi, Y.; Harasawa, A.; Yaji, K.; Shirasawa, T.; Nittoh, K.; Yang, W.; Miki, K.; Oda, T.; Yeom, H. W.; Sakamoto, K. Nonvortical Rashba spin structure on a surface with C_{1h} symmetry. *Phys. Rev. Lett.* **2016**, *117*, 016803.
(42) Ichinokura, S.; Bondarenko, L. V.; Tupchaya, A. Y.; Gruznev, D. V.; Zotov, A. V.; Saranin, A. A.; Hasegawa, S. Superconductivity in thallium double atomic layer and transition into an insulating phase intermediated by a quantum metal state. *2D Mater.* **2017**, *4*, 025020.
(43) Yamada, M.; Hirahara, T.; Hobara, R.; Hasegawa, S.; Mizuno, H.; Miyatake, Y.; Nagamura, T. Surface electrical conductivity measurement system with micro-four-point probes at sub-Kelvin temperature under high magnetic field in ultrahigh vacuum. *e-J. Surf. Sci. Nanotechnol.* **2012**, *10*, 400−405.
(44) Rawlings, K. J.; Gibson, M. J.; Dobson, P. J. The epitaxial growth of lead and thallium on (111) silver and copper. *J. Phys. D: Appl. Phys.* **1978**, *11*, 2059−2070.
(45) Toney, M. F.; Gordon, J. G.; Samant, M. G.; Borges, G. L.; Melroy, O. R.; Yee, D.; Sorensen, L. B. Underpotentially deposited thallium on silver (111) by in situ surface x-ray scattering. *Phys. Rev. B* **1992**, *45*, 9362−9374.
(46) He, S.; He, J.; Zhang, W.; Zhao, L.; Liu, D.; Liu, X.; Mou, D.; Ou, Y.-B.; Wang, Q.-Y.; Li, Z.; Wang, L.; Peng, Y.; Liu, Y.; Chen, C.; Yu, L.; Liu, G.; Dong, X.; Zhang, J.; Chen, C.; Xu, Z.; Chen, X.; Ma, X.; Xue, Q.; Zhou, X. J. Phase diagram and electronic indication of high-temperature superconductivity at 65 K in single-layer FeSe films. *Nat. Mater.* **2013**, *12*, 605−610.
(47) Ge, J.-F.; Liu, Z.-L.; Liu, C.; Gao, C.-L.; Qian, D.; Xue, Q.-K.; Liu, Y.; Jia, J.-F. Superconductivity above 100 K in single-layer FeSe films on doped $SrTiO_3$. *Nat. Mater.* **2015**, *14*, 285−289.

Recommended by ACS

Giant and Tunable Out-of-Plane Spin Polarization of Topological Antimonene

Polina M. Sheverdyaeva, Paolo Moras, *et al.*

JULY 17, 2023
NANO LETTERS
READ

Controlling the Interlayer Dzyaloshinskii–Moriya Interaction by Electrical Currents

Fabian Kammerbauer, Mathias Kläui, *et al.*

JULY 19, 2023
NANO LETTERS
READ

Experimental Demonstration of a Magnetically Induced Warping Transition in a Topological Insulator Mediated by Rare-Earth Surface Dopants

Beatriz Muñiz Cano, Miguel A. Valbuena, *et al.*

MAY 08, 2023
NANO LETTERS
READ

Influence of Magnetic and Electric Fields on Universal Conductance Fluctuations in Thin Films of the Dirac Semimetal Cd_3As_2

Run Xiao, Nitin Samarth, *et al.*

JUNE 15, 2023
NANO LETTERS
READ

Get More Suggestions >

https://doi.org/10.1021/acs.nanolett.3c02387
Nano Lett. 2023, 23, 7675−7682